Research Article

Degenerated-Inverse-Matrix-Based Channel Estimation for OFDM Systems

Makoto Yoshida

Fujitsu Laboratories Limited, YRP R&D Center , 5-5, Hikari-no-Oka, Yokosuka, 239-0847, Japan

Correspondence should be addressed to Makoto Yoshida, mako@labs.fujitsu.com

This paper addresses time-domain channel estimation for pilot-symbol-aided orthogonal frequency division multiplexing (OFDM) systems. By using a cyclic sinc-function matrix uniquely determined by N_c transmitted subcarriers, the performance of our proposed scheme approaches perfect channel state information (CSI), within a maximum of 0.4 dB degradation, regardless of the delay spread of the channel, Doppler frequency, and subcarrier modulation. Furthermore, reducing the matrix size by splitting the dispersive channel impulse response into clusters means that the degenerated inverse matrix estimator (DIME) is feasible for broadband, high-quality OFDM transmission systems. In addition to theoretical analysis on normalized mean squared error (NMSE) performance of DIME, computer simulations over realistic nonsample spaced channels also showed that the DIME is robust for intersymbol interference (ISI) channels and fast time-invariant channels where a minimum mean squared error (MMSE) estimator does not work well.

1. Introduction

Orthogonal frequency division multiplexing (OFDM) is well known as an anti-multipath-fading technique for broadband wireless systems and is used as a standard in digital broadcasting and wireless LAN systems. Increased demand for a better broadband wireless system—a fourth-generation (4G) mobile system—has stemmed from the use of this technique [1].

Coherent OFDM detection requires the channel state information (CSI) to be estimated accurately because signals received over a multipath fading channel have unknown amplitude and phase variations. Known pilot symbols are therefore inserted into the transmitted data stream periodically and channel estimation is performed by interpolating them.

Various pilot-symbol-aided channel estimation schemes have been investigated for OFDM [2–4] and multiinput-multioutput (MIMO) OFDM systems [5, 6]. OFDM with high-order modulation schemes, such as multilevel QAM (M-QAM), requires more accurate channel estimation than does OFDM with PSK modulation because it is more sensitive to noise. An adaptive OFDM technique [7] uses

M-QAM and is essential for highly efficient communications. OFDM systems with multiple transmitting antennas, including MIMO-OFDM systems, also need accurate channel estimation. When different signals are transmitted from different transmit antennas simultaneously, the received signal can be considered as the superposition of these signals, which have higher-order signal constellations than does the original signal.

The minimum mean squared error (MMSE) estimator has been proposed as an optimal solution for a pilot-symbol-aided channel estimation scheme [8]. The MMSE estimator, however, requires huge computational resources, and the performance deteriorates significantly for fast time-invariant channels where the convergence algorithm cannot work well within the observation duration.

Our proposed scheme uses a cyclic sinc-function matrix uniquely determined by N_c transmitted subcarriers. Since this sinc-function ("time response of a subcarrier" in a broad sense) is a deterministic and known vector, the inverse matrix (IM) approach can be used for high-precision estimation without supplementary information such as knowledge of the channel statistics and operating SNR, which are required in the MMSE estimator.

Time-domain channel estimators have problems of energy leakage over nonsample spaced channels [5, 8, 9] and high computational complexity. Our proposed scheme solves not only these two problems but also that of residual noise by introducing a degenerated inverse matrix (DIM) and oversampling technique simultaneously.

This paper shows that the degenerated inverse matrix estimator (DIME) can estimate CSI in a fast-fading environment almost perfectly no matter what the subcarrier modulation scheme and delay spread of the channel are. In Section 2 we describe the system model, and in Section 3 we discuss DIME, comparing it with other estimators based on zero-forcing (ZF), ZF with averaging in the frequency domain (ZF-FAV) [1], and MMSE. In Section 4 we compare these techniques in terms of computational complexity and performance, including theoretical analysis on normalized mean squared error (NMSE) performance of DIME through computer simulations under the specifications that we assumed for 4G mobile systems. Our conclusions are given in Section 5.

2. System Description

Figure 1 shows the frame format for OFDM signals. The data symbols are time-multiplexed with the pilot symbols. This time-division-multiplexing (TDM) type of pilot symbol is used in the 4G system proposed by Atarashi et al. [1].

Thus, in this paper, pilot symbols mapped over all subcarriers are interpolated only in the time direction. We assume that T_S is the sampling interval and that a guard interval (GI) of time length T_G is used to eliminate intersymbol interference (ISI). Thus the OFDM symbol duration is $T = NT_S + T_G$, where N is the size of the fast Fourier transform (FFT) used in the system.

Consider the OFDM system shown in Figure 2, where x_n are the transmitted symbols, $g(t)$ is the channel impulse response (CIR), $\widetilde{w}(t)$ is the additive white Gaussian noise (AWGN), and y_n are the received symbols. In this system the transmitted symbols x_n ($0 \leq n \leq N_c - 1$) assigned to N_c subcarriers are fed into an N-point ($N_c < N$) inverse FFT, where N-N_c subcarriers (virtual carriers) are not used at the edges of the spectrum to avoid aliasing problems at the receiver. Note that in this paper, $\mathbf{FFT}_N$ and $\mathbf{IFFT}_N$, respectively, denote an N-point FFT and N-point inverse FFT given by

$$\mathbf{FFT}_N(\mathbf{x}) = \frac{1}{\sqrt{N}} \sum_{k=0}^{N-1} x(k)e^{-j2\pi kn/N},$$

$$\mathbf{IFFT}_N(\mathbf{x}) = \frac{1}{\sqrt{N}} \sum_{n=0}^{N-1} x(n)e^{j2\pi kn/N}. \tag{1}$$

The CIR is expressed by

$$g(t) = \sum_{l=0}^{L-1} \alpha_l \delta(t - \tau_l), \tag{2}$$

where L is the total path number and α_l and τ_l are the complex amplitude and time delay of the lth path. Thus we
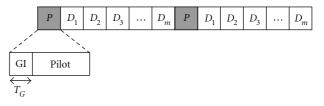

FIGURE 1: OFDM system frame format.

can say that the maximum excess delay $\tau_{\max} = \tau_{L-1}$. We also assume that the entire CIR lies inside the guard interval, that is, $0 \leq \tau_{\max} \leq T_G$. Therefore, the cyclic convolution of the received sequence over the FFT window is preserved. The N-dimensional received symbol vector

$$\mathbf{y} = \begin{bmatrix} y_0 \cdots y_{N_c/2-1} \ y_{N_c/2} \cdots y_{N-N_c/2-1} \ y_{N-N_c/2} \ \cdots \ y_{N-1} \end{bmatrix}^T \tag{3}$$

is given as

$$\mathbf{y} = \mathbf{FFT}_N \left[\mathbf{IFFT}_N(\mathbf{x}) \otimes \frac{\mathbf{g}}{\sqrt{N}} + \widetilde{\mathbf{w}} \right], \tag{4}$$

where $\otimes$ denotes cyclic convolution. The N-dimensional transmitted symbol vector with N-N_c zeros, the CIR vector after sampling of $g(t)$, and the AWGN vector after sampling of $\widetilde{w}(t)$ are, respectively, given by

$$\mathbf{x} = \begin{bmatrix} x_0 & \cdots & x_{N_c/2-1} \ 0 & \cdots & 0 & x_{N-N_c/2} & \cdots & x_{N-1} \end{bmatrix}^T,$$

$$\mathbf{g} = \begin{bmatrix} g_0 \ g_1 \ \cdots \ g_{N-1} \end{bmatrix}^T,$$

$$\widetilde{\mathbf{w}} = \begin{bmatrix} \widetilde{w}_0 \ \widetilde{w}_1 \ \cdots \ \widetilde{w}_{N-1} \end{bmatrix}^T \tag{5}$$

(the superscript $[\cdot]^T$ indicates vector transpose). Note that y_n ($N_c/2 \leq n \leq N - N_c/2 - 1$) are discarded at the receiver as virtual subcarriers.

The kth element of vector $\mathbf{g}$ can be expressed by

$$g_k = \frac{1}{\sqrt{N}} \sum_{l=0}^{L-1} \alpha_l e^{-j(\pi/N)(k+(N-1)\tau_l/T_S)} \cdot \frac{\sin(\pi\tau_l/T_S)}{\sin((\pi/N)(\tau_l/T_S - k))}. \tag{6}$$

Equation (6) indicates that if τ_l/T_S is not an integer, the energy will leak to all taps g_k. This is a serious problem for the time-domain channel estimator. Furthermore, the time response (*sinc function* in our system) of an OFDM signal with virtual carriers leaks to all taps, superposed on the leakage of (6).

We can rewrite the right-hand side of (4) in matrix notation [8] as follows:

$$\mathbf{y} = \mathbf{X}\mathbf{F}_N\mathbf{g} + \mathbf{w}, \tag{7}$$

where $\mathbf{X}$ is the N-dimensional diagonal matrix

$$\mathbf{X} = \text{diag}\begin{pmatrix} x_0 \cdots x_{N_c/2-1} \ 0 \cdots 0 \ x_{N-N_c/2} \ \cdots \ x_{N-1} \end{pmatrix}, \tag{8}$$

$\mathbf{F}_N$ is an $N \times N$-dimensional FFT matrix with entries

$$[\mathbf{F}_N]_{k,n} = \frac{1}{\sqrt{N}} e^{-j2\pi kn/N} \quad 0 \leq k, n \leq N - 1, \tag{9}$$

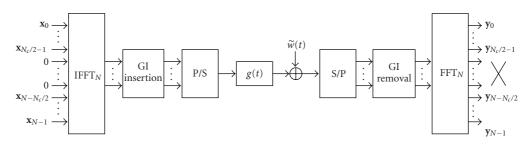and $\mathbf{w} = \mathbf{F}_N\widetilde{\mathbf{w}}$.

FIGURE 2: Block diagram of OFDM system.

3. Channel Estimation

We describe several estimators based on the system model described in the previous section. The goal is to derive estimates of the channel transfer function (CTF) $\mathbf{h}$, which is the Fourier transform of the CIR. That is, $\mathbf{h} = \mathbf{F}_N \mathbf{g}$.

Note that in pilot-symbol-aided channel estimation, since a pilot symbol is used only as a known transmitted symbol, the receiver can easily estimate the CTF in the frequency domain.

3.1. ZF and ZF-FAV Estimators. The ZF estimator, or least square (LS) estimator, uses the pilot symbol sequence to generate the estimated CTF

$$\hat{\mathbf{h}}_{\mathrm{ZF}} = \mathbf{Z}\mathbf{y} = \mathbf{Z}(\mathbf{X}\mathbf{F}_N\mathbf{g} + \mathbf{w}) = \mathbf{Z}\mathbf{X}\mathbf{F}_N\mathbf{g} + \mathbf{Z}\mathbf{w}, \qquad (10)$$

where $\mathbf{Z}$ is the N-dimensional diagonal matrix

$$\mathbf{Z} = \mathrm{diag}\Big(1/x_0 \cdots 1/x_{N_c/2-1}\ 0 \cdots 0 1/x_{N-N_c/2} \cdots 1/x_{N-1}\Big),$$

$$\mathbf{Z}\mathbf{X} = \mathrm{diag}\Big(1 \cdots 1 0 \cdots 0 1 \cdots 1\Big), \qquad (11)$$

and the second term is the residual noise term of ZF.

The ZF-FAV estimator [1] uses the CTF averaged over the adjacent $2D + 1$ subcarriers in the frequency domain for noise suppression. This averaging process is done after getting the CTF for each subcarrier. The estimated CTF at the nth subcarrier ($0 \le n \le N_c/2 - 1, N - N_c/2 \le n \le N - 1$) is given by

$$\hat{h}_{ZF-FAV}(n) = \begin{cases} \dfrac{1}{2D+1} \displaystyle\sum_{d=(n-D+N)\bmod N}^{(n+D)\bmod N} \hat{h}_{ZF}(d) \\ \quad 0 \le n < \dfrac{N_c}{2} - D, N - \dfrac{N_c}{2} + D \le n < N, \\[2pt] \dfrac{1}{(N_c/2)-n-D} \displaystyle\sum_{d=(n-D+N)\bmod N}^{(N_c/2)-1} \hat{h}_{ZF}(d) \\ \quad \dfrac{N_c}{2} - D \le n < \dfrac{N_c}{2}, \\[2pt] \dfrac{1}{n-(N-N_c/2)+D+1} \displaystyle\sum_{d=N-N_c/2}^{(n+D)\bmod N} \hat{h}_{ZF}(d) \\ \quad N - \dfrac{N_c}{2} \le n < N - \dfrac{N_c}{2} + D. \end{cases}$$

$$(12)$$

Since this algorithm employs the property of a coherent bandwidth, its performance degrades when the channel has a large delay spread.

3.2. MMSE Estimator. The MMSE estimator is proposed as an optimum solution for pilot-symbol-aided channel estimation. If the vector $\mathbf{g}$ is uncorrelated with the vector $\mathbf{w}$, the estimated CTF is given by [8]

$$\hat{\mathbf{h}}_{\mathrm{MMSE}} = \mathbf{F}_N \mathbf{R}_{\mathbf{gy}} \mathbf{R}_{\mathbf{yy}}^{-1} \mathbf{y}, \qquad (13)$$

where

$$\mathbf{R}_{\mathbf{gy}} = \mathrm{E}\big\langle \mathbf{g}\mathbf{y}^{\mathrm{H}} \big\rangle = \mathbf{R}_{\mathbf{gg}} \mathbf{F}_N^{\mathrm{H}} \mathbf{X}^{\mathrm{H}},$$

$$\mathbf{R}_{\mathbf{yy}} = \mathrm{E}\big\langle \mathbf{y}\mathbf{y}^{\mathrm{H}} \big\rangle = \mathbf{X}\mathbf{F}_N \mathbf{R}_{\mathbf{gg}} \mathbf{F}_N^{\mathrm{H}} \mathbf{X}^{\mathrm{H}} + \sigma^2 \mathbf{I}_N \qquad (14)$$

($[\cdot]^{\mathrm{H}}$ and $\mathbf{I}_N$ indicate a Hermitian matrix and an $N \times N$-dimensional identity matrix, resp.).

Since (13) requires the autocovariance matrix of $\mathbf{g}$, $\mathbf{R}_{\mathbf{gg}} = \mathrm{E}\langle \mathbf{g}\mathbf{g}^{\mathrm{H}} \rangle$, and the noise variance, $\sigma^2 = \mathrm{E}\langle |w_i|^2 \rangle$, this algorithm is not suitable for a fast-fading environment where these two quantities cannot be converged.

To solve the problem of high computational complexity, a modification of the MMSE has been proposed [8]. The modified MMSE reduces the size of $\mathbf{R}_{\mathbf{gg}}$ by considering a given area, for example, the number of taps in a guard interval.

3.3. DIM Estimator (DIME). The proposed estimator, DIME, which is based on time-domain signal processing, solves not only the problems of energy leakage and computational complexity but also that of residual noise, by introducing a degenerated inverse matrix and oversampling technique.

The zero-insertion CTF for M-fold oversampling is first formed by inserting MN-N_c zeros in the middle frequency indices:

$$\hat{\mathbf{h}}_{\mathrm{ZF}}^{\smile} = \begin{cases} \hat{h}_{\mathrm{ZF}}(n) & 0 \le n < N_c/2, \\ 0 & N_c/2 \le n < MN - N_c/2, \\ \hat{h}_{\mathrm{ZF}}(n - (M-1)N) & MN - N_c/2 \le n < MN, \end{cases}$$

$$(15)$$

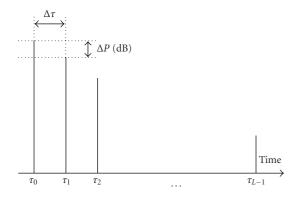where the superscript $\smile$ denotes oversampling.

FIGURE 3: Channel model with exponential decay paths.

Then the oversampled CIR is solved after calculating the IFFT of $\hat{\tilde{\mathbf{h}}}_{ZF}$:

$$\hat{\tilde{\mathbf{g}}}_{ZF} = \mathbf{F}_{MN}^{H}\hat{\tilde{\mathbf{h}}}_{ZF} = \mathbf{S}\breve{\mathbf{g}} + \breve{\tilde{\mathbf{w}}}, \qquad (16)$$

where $\breve{\tilde{\mathbf{w}}} = \mathbf{F}_{MN}^{H}\breve{\mathbf{w}}$, and the time-response matrix $\mathbf{S}$ is given by

$$\mathbf{S} = \mathbf{F}_{MN}^{H}\breve{\mathbf{Z}}\breve{\mathbf{X}}\mathbf{F}_{MN}. \qquad (17)$$

Using the inverse matrix, $\mathbf{S}^{-1}$, which is a definitive and known matrix, the IM estimator generates

$$\hat{\tilde{\mathbf{g}}}_{IM} = \mathbf{S}^{-1}\hat{\tilde{\mathbf{g}}}_{ZF} = \mathbf{S}^{-1}(\mathbf{S}\breve{\mathbf{g}} + \breve{\tilde{\mathbf{w}}}) = \breve{\mathbf{g}} + \mathbf{S}^{-1}\breve{\tilde{\mathbf{w}}}. \qquad (18)$$

Next, we degenerate $\mathbf{S}$ to reduce the size of the matrix and suppress residual noise.

A property of the time-response matrix $\mathbf{S}$ formed by the cyclic sinc-function is that significant energy is concentrated in the diagonal elements. Since the correlation between $\breve{\mathbf{g}}$ and $\breve{\mathbf{g}}_{ZF}$ is high, we can form the degenerated inverse matrix $\mathbf{S'}^{-1}$ as follows. First, in (16), we discard the kth sample $\hat{\tilde{\mathbf{g}}}_{ZF}(k)$ with lower energy than a given threshold, the corresponding $\breve{\mathbf{g}}(k)$, and the corresponding noise term $\breve{\tilde{\mathbf{w}}}(k)$. Next, the matrix size of $\mathbf{S}$ is reduced by generating a submatrix $\mathbf{S'}$ in which both the row and column corresponding to the discarded samples are eliminated. If the shape of the CIR is cluster-like, multiple degenerated inverse matrices can be generated on a cluster-by-cluster basis. This significantly reduces the computational complexity (evaluated quantitatively in Section 4).

The degenerated $\hat{\tilde{\mathbf{g}}}_{ZF}$ is given as

$$\hat{\tilde{\mathbf{g}}}_{ZF}' = \mathbf{S'}\breve{\mathbf{g}}\prime + \breve{\tilde{\mathbf{w}}}', \qquad (19)$$

and we get

$$\hat{\tilde{\mathbf{g}}}_{DIM}' = \mathbf{S'}^{-1}\hat{\tilde{\mathbf{g}}}_{ZF}' = \hat{\tilde{\mathbf{g}}}' + (\breve{\mathbf{X}}'\mathbf{F}_{MN}')^{-1}\mathbf{F}_{MN}'\breve{\tilde{\mathbf{w}}}'. \qquad (20)$$

Then the MN-dimensional (full size) vector $\breve{\mathbf{g}}_{DIM}$ is reformed by zero-padding all the discarded samples. Zero-padding also has the function of suppressing residual noise.

By calculating the FFT of $\hat{\tilde{\mathbf{g}}}_{DIM}'$, the DIME generates

$$\hat{\tilde{\mathbf{h}}}_{DIM} = \mathbf{F}_{MN}\hat{\tilde{\mathbf{g}}}_{DIM}, \qquad (21)$$

and then the T_S-sampled CTF is given as

$$\hat{\mathbf{h}}_{DIM} = \begin{cases} \hat{\tilde{h}}_{DIM}(n) & 0 \le n < N_c/2, \\ \hat{\tilde{h}}_{DIM}(n + (M-1)N) & N - N_c/2 \le n < N. \end{cases} \qquad (22)$$

4. Performance Evaluation

4.1. System Parameters. The main simulation parameters assumed for a broadband mobile communications system are listed in Table 1. We assumed that both symbol-time and sample-time were synchronized perfectly.

We then examined the BER performance using a general L-ray Rayleigh fading channel with exponential decay paths (Figure 3). The average received power of the lth path decreased by $(l \times \Delta P)$ dB relative to the first path, where $l = 0, 1, \ldots, L - 1$. We set $\Delta P = 1$ and $L = 12$. The path interval was given as $\Delta\tau = \tau_i - \tau_{i-1}$. In this simulation, we defined a tapped-delay-line channel model for a nonsample spaced channel with a tap interval of $T_S/4$ and a first tap delay of $\tau_0 = T_S/4$. This channel model was used to evaluate the worst case for the DIME with two-fold oversampling (M=2).

4.2. Complexity Analysis. We first analyze the computational complexity of the channel estimators described in Section 3. We assume that the complexity is the sum of the number of complex multiplications, complex divisions, and complex additions. Table 2 shows the computational complexity for five algorithms.

The main complexity of the ZF estimator is 1024-point FFT operation. The ZF-FAV estimator requires 3-subcarrier averaging in addition to that of the ZF estimator. Since these estimators do not require time-domain processing, they have very low complexity.

The main complexity of the MMSE-based estimator is the inverse matrix operation. In this paper, we assume that the autocovariance matrix $\mathbf{R_{gg}}$ is calculated on a pilot–by-pilot basis to follow fast time-invariant channels and the noise variance is assumed to be known. The size of the degenerated autocovariance matrix $\mathbf{R_{gg}}$ for the modified MMSE estimator is set as 220×220 ($\approx T_G \times T_G$). Since our parameters require a very large matrix for the MMSE, this level of complexity is unfeasible and we discarded the full-MMSE from the performance comparison.

For the inverse matrix operation, the DIME with M=2 needs to calculate two complex FFT operations: $2N$-point IFFT and FFT. Although the FFT is required to be large, the resulting complexity is very small because the DIM technique is used. Using the threshold for DIM, the 2048×2048 full matrix was degenerated to a 43×43-dimensional matrix. The complexity of the DIME is 8.6 times that of the ZF and 1/20000 that of MMSE estimators.

4.3. MSE Performance. We then examined the NMSE [10] performance as a function of E_b/N_0 in two different channel

TABLE 1: Simulation parameters.

Sampling frequency	78.336 MHz
Number of subcarriers	896 ($N = 1024$)
Subcarrier spacing	76.5 kHz
Symbol duration	$T = 15.63\mu s$
GI duration	$T_G = 2.55\mu s$ ($= 200T_S$)
Frame length	28 Data + 2 Pilot ($=0.47$ ms)
Transmission rate	106.8 Mb/s, 160.4 Mb/s
Modulation	16 QAM, 64 QAM
Channel coding/decoding	Turbo coding ($R = 1/2, k = 4$)/
(FEC)	Max-Log-MAP decoding (Iterations=8)
Channel interleaving	Random interleaving
Interpolation in time direction	First order linear interpolation
Oversampling for DIM	M=2
Threshold for DIM	-16 dB from the sample with most significant energy
Averaging for ZF-FAV	D=1 [1]
Rx antenna diversity	2-branch MRC

TABLE 2: Computational complexity.

Algorithm	Computational complexity
DIME ($M = 2$)	1.40×10^5
ZF	1.63×10^4
ZF-FAV ($D = 1$)	1.98×10^4
MMSE	2.87×10^9
Modified MMSE	2.89×10^7

models that included paths within ($\sigma/T = 0.043$) and beyond GI ($\sigma/T = 0.123$).

NMSE performances with $\sigma/T = 0.043$ ($\sigma = 0.67\mu s$) are shown in Figure 4. The normalized rms delay spreads of $\sigma/T = 0.043$ correspond to $\tau_{\max} \approx T_G$. The maximum Doppler frequency $f_d = 480$ Hz, corresponding to the normalized Doppler frequency of $f_dT = 0.0075$, was also examined. In a within-GI case without the occurrence of ISI, we can get the analytical NMSE in a relatively easy way. The analytical NMSEs for DIM and ZF estimator are thus plotted simultaneously.

Analytical NMSE for DIM estimator, $NMSE_{\text{DIM}}$, is given as

$$NMSE_{\text{DIM}} = \frac{\left\{\sum_{n=0}^{N_c/2-1} \left|\left[\mathbf{F}'_{MN}\hat{\breve{\mathbf{g}}}'\right]_n - \left[\mathbf{F}_{MN}\breve{\mathbf{g}}\right]_n\right|^2\right\}}{N_c}$$
$$+ \frac{\left\{\sum_{n=N-N_c/2}^{N-1} \left|\left[\mathbf{F}'_{MN}\hat{\breve{\mathbf{g}}}'\right]_n - \left[\mathbf{F}_{MN}\breve{\mathbf{g}}\right]_n\right|^2\right\}}{N_c}$$
$$+ \frac{\lambda}{MN}\sigma^2,$$
(23)

where $[\cdot]_n$ denotes the nth element of a vector, λ is the number of the samples greater than a given threshold (see Appendix A). In (23), $\hat{\breve{\mathbf{g}}}'$ and λ were previously given by going through simple simulation.

Analytical NMSE for ZF estimator, $NMSE_{ZF}$, is also given as

$$NMSE_{ZF} = \sigma^2,$$
(24)

(see Appendix B). The noise suppression gain by the first order linear interpolation, -1.9 dB, was also considered (see Appendix C).

We can see that the analytical results are in excellent agreement with the computational simulation results. The slight differences in ZF at higher E_b/N_0 and in DIME at lower E_b/N_0 are due to the channel estimation error ($= \varepsilon$), which is not considered in the assumption.

For the former case, since the NMSE performance of ZF depends only on E_b/N_0 ($= \sigma^2$), we can see the effect of channel estimation error at higher E_b/N_0, where $\sigma^2 < \varepsilon$. For the latter case, since λ is independent of E_b/N_0, we can see the effect of erroneous selection of effective samples at lower E_b/N_0.

Next, NMSE performances with $\sigma/T = 0.123$ ($\sigma = 1.92\mu s$), $\tau_{\max} \approx 3T_G$ are shown in Figure 5. The DIME performs well at the target E_b/N_0 lower than 10 dB (Figures 6 and 7), regardless of the channel model since it has a powerful noise suppression capability. The modified MMSE estimator works well only in both a high E_b/N_0 and within-GI environment that can generate $\mathbf{R_{gg}}$ accurately on a pilot-by-pilot basis. Based on computational complexity and performance, three estimators other than the modified MMSE estimator are examined in the following sections.

4.4. Performance in Modulation Scheme. We examined the BER performance as a function of E_b/N_0 in two different subcarrier modulation schemes: 16 QAM and 64 QAM.

BER performances with 16-QAM-OFDM and 64-QAM-OFDM are shown in Figures 6 and 7, respectively. $\sigma/T = 0.043$ and $f_dT = 0.0075$ were examined.
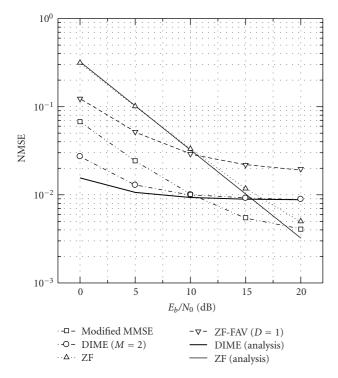
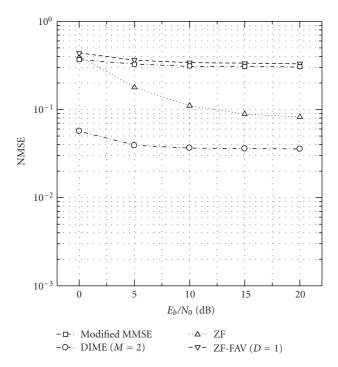FIGURE 4: NMSE performance with $\sigma/T = 0.043$ and $f_d T = 0.0075$.

FIGURE 6: BER performance with 16-QAM-OFDM.

FIGURE 5: NMSE performance with $\sigma/T = 0.123$ and $f_d T = 0.0075$.
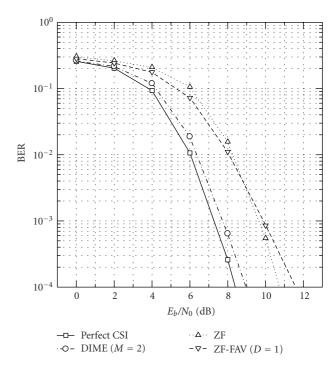

FIGURE 7: BER performance with 64-QAM-OFDM.

We can see that the DIME achieved a good performance for 16-QAM-OFDM, degradation within 0.2 dB (compared to perfect CSI), and for 64-QAM-OFDM, degradation within 0.4 dB, even in a nonsample spaced channel. The frequency-domain estimators, both ZF and ZF-FAV, were obviously not sensitive to the chosen nonsample tap position. The subcarrier averaging in the frequency domain, employed for ZF-FAV, had a certain effect on 16-QAM-OFDM but had no effect on 64-QAM-OFDM. For 16-QAM-OFDM the performance gain of the DIME relative to ZF-FAV was almost
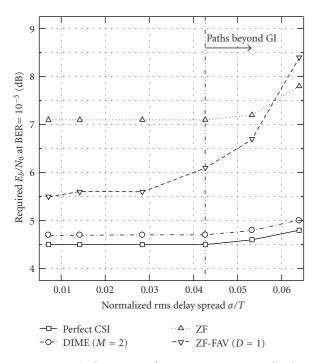
FIGURE 8: Required E_b/N_0 performance versus normalized rms delay spread with $f_d T = 0.0075$ (16-QAM-OFDM).

FIGURE 9: Required E_b/N_0 performance versus normalized rms delay spread with $f_d T = 0.0075$ (64-QAM-OFDM).

1.5 dB at a BER of 10^{-3}, and for 64-QAM-OFDM it was more than 2.0 dB at a BER of 10^{-3}.

4.5. Performance in Delay Spread. We next examined the relation between a normalized rms delay spread σ/T and the average received E_b/N_0 performance needed for an average BER of 10^{-3}.

The effects of the delay spread in different channel estimators with 16-QAM-OFDM and 64-QAM-OFDM are shown in Figures 8 and 9, respectively. A normalized Doppler frequency of $f_d T = 0.0075$ was examined and the delay spread was varied by changing $\Delta\tau$ in the channel model depicted in Figure 3. Although ZF-FAV performed well when the delay spread was small, its performance deteriorated significantly as the delay spread increased, or the coherent bandwidth became narrower. Also in this situation, the DIME performance was maintained regardless of the delay spread of the channel, even in ISI channels with $\sigma/T > 0.043$, where a delayed path occurs beyond the GI.

4.6. Performance in Doppler Frequency. We examined the relation between the normalized Doppler frequency $f_d T$ and the average received E_b/N_0 performance needed for an average BER of 10^{-3}.

The effects of the normalized Doppler frequency on different channel estimators with 16-QAM-OFDM and 64-QAM-OFDM are shown in Figures 10 and 11, respectively. A normalized delay spread of $\sigma/T = 0.043$ was examined and the maximum Doppler frequency, f_d, was changed from 64 Hz to 480 Hz, corresponding to a vehicle speed of 14 km/h to 104 km/h at a carrier frequency of 5 GHz. The
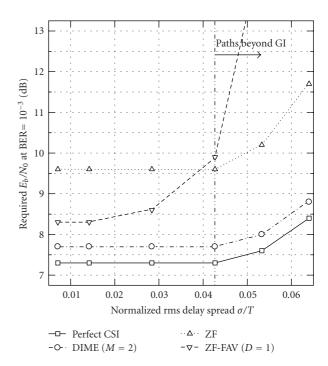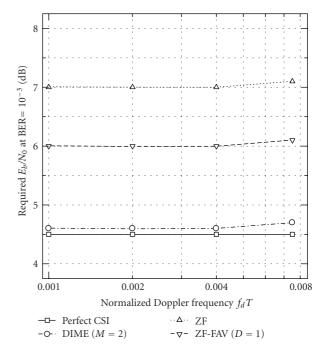

FIGURE 10: Required E_b/N_0 performance versus normalized Doppler frequency with $\sigma/T = 0.043$ (16-QAM-OFDM).

performance of all channel estimators was maintained from low to high Doppler frequencies because they do not require any channel statistics that need a specific time coherency, such as averaging in the time direction. The DIME is also a decision-directed estimator operating on a pilot–by–pilot basis.
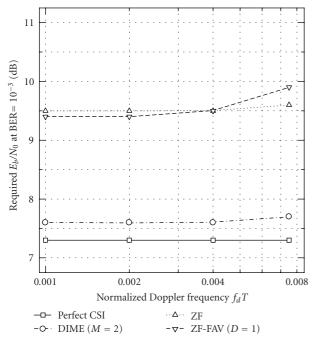
Figure 11: Required E_b/N_0 performance versus normalized Doppler frequency with $\sigma/T = 0.043$ (64-QAM-OFDM).

5. Conclusion

This paper described a novel channel estimation scheme for OFDM systems. The proposed channel estimator, DIME, uses a cyclic sinc-function matrix that is uniquely determined by N_c transmitted subcarriers and is composed of a deterministic and known vector. The computational complexity required for time-domain processing was reduced by taking a submatrix approach. Our setup reduced the matrix size by 1/20000 compared to the MMSE estimator.

For realistic nonsample spaced channels, including ISI channels, the DIME performed very well—yielding nearly the actual CSI—regardless of the delay spread, Doppler frequency, and subcarrier modulation scheme. We also showed that an oversampling size of $M = 2$ for the DIME was sufficient to maintain this performance in arbitrary nonsample spaced channel models.

Appendices

A. NMSE for DIM Estimator

The normalized mean squared error (NMSE) is generally given by

$$
\text{NMSE} = \frac{\text{E}\left\{\sum_{n=0}^{N_c/2-1}\left|\hat{h}_n - h_n\right|^2 + \sum_{n=N-N_c/2}^{N-1}\left|\hat{h}_n - h_n\right|^2\right\}}{\text{E}\left\{\sum_{n=0}^{N_c/2-1}|x_n|^2 + \sum_{n=N-N_c/2}^{N-1}|x_n|^2\right\}},
\tag{A.1}
$$

where $\hat{\mathbf{h}}$ is the N-dimensional estimated CTF vector and $\text{E}\{\cdot\}$ denotes the expectation operator.

The CTF of DIM estimator is redefined as

$$
\hat{\mathbf{h}}_{\text{DIM}} = \begin{cases} \hat{\bar{h}}_{\text{DIM}}(n) & 0 \le n < N_c/2, \\ \hat{\bar{h}}_{\text{DIM}}(n + (M-1)N) & N - N_c/2 \le n < N, \end{cases}
\tag{A.2}
$$

where

$$
\hat{\bar{\mathbf{h}}}_{\text{DIM}} = \mathbf{F}_{MN}\hat{\bar{\mathbf{g}}}_{\text{DIM}},
\tag{A.3}
$$

and $\breve{\mathbf{g}}_{\text{DIM}}$ is reformed by zero-padding all the discarded samples of

$$
\hat{\bar{\mathbf{g}}}'_{\text{DIM}} = \mathbf{S}'^{-1}\hat{\bar{\mathbf{g}}}'_{\text{ZF}} = \hat{\bar{\mathbf{g}}}' + \left(\breve{\mathbf{X}}'\mathbf{F}'_{MN}\right)^{-1}\mathbf{F}'_{MN}\breve{\mathbf{w}}'.
\tag{A.4}
$$

From (A.1) to (A.4), NMSE for DIM estimator is given as

$$
\text{NMSE}_{\text{DIM}} = \frac{\text{E}\left\{\sum_{n=0}^{N_c/2-1}\left|\left[\hat{h}_{\text{DIM}}\right]_n - [h]_n\right|^2\right\}}{N_c}
$$
$$
+ \frac{\text{E}\left\{\sum_{n=N-N_c/2}^{N-1}\left|\left[\hat{h}_{\text{DIM}}\right]_n - [h]_n\right|^2\right\}}{N_c}
\tag{A.5}
$$

The first term in (A.5) is derived as

$$
\frac{\text{E}\left\{\sum_{n=0}^{N_c/2-1}\left|\left[\hat{h}_{\text{DIM}}\right]_n - [h]_n\right|^2\right\}}{N_c} = \frac{\text{E}\left\{\sum_{n=0}^{N_c/2-1}\left|\left[\mathbf{F}_{MN}\hat{\bar{\mathbf{g}}}_{\text{DIM}}\right]_n - [\mathbf{F}_{MN}\breve{\mathbf{g}}]_n\right|^2\right\}}{N_c}
$$
$$
= \frac{\text{E}\left\{\sum_{n=0}^{N_c/2-1}\left|\left[\mathbf{F}'_{MN}\hat{\bar{\mathbf{g}}}' + \mathbf{F}'_{MN}\left(\breve{\mathbf{X}}'\mathbf{F}'_{MN}\right)^{-1}\mathbf{F}'_{MN}\breve{\mathbf{w}}'\right]_n - [\mathbf{F}_{MN}\breve{\mathbf{g}}]_n\right|^2\right\}}{N_c}
\tag{A.6}
$$
$$
= \frac{\text{E}\left\{\sum_{n=0}^{N_c/2-1}\left|\left[\mathbf{F}'_{MN}\hat{\bar{\mathbf{g}}}'\right]_n - [\mathbf{F}_{MN}\breve{\mathbf{g}}]_n\right|^2\right\}}{N_c} + \frac{\lambda}{2MN}\sigma^2,
$$

where $[\cdot]_n$ denotes the nth element of a vector, λ is the number of the samples greater than a given threshold. Since the second term in (A.5) can also be derived similarly, NMSE for DIM estimator is defined as (A.7) In (A.7), the first term and the second term are channel estimation errors, and the third term is the residual noise.

$$
\begin{aligned}
\mathrm{NMSE}_{\mathrm{DIM}} = {} & \frac{\mathrm{E}\left\{\sum_{n=0}^{N_c/2-1}\left|\left[\mathbf{F}'_{MN}\hat{\breve{\mathbf{g}}}'\right]_n - \left[\mathbf{F}_{MN}\breve{\mathbf{g}}\right]_n\right|^2\right\}}{N_c} \\
& + \frac{\mathrm{E}\left\{\sum_{n=N-N_c/2}^{N-1}\left|\left[\mathbf{F}'_{MN}\hat{\breve{\mathbf{g}}}'\right]_n - \left[\mathbf{F}_{MN}\breve{\mathbf{g}}\right]_n\right|^2\right\}}{N_c} \\
& + \frac{\lambda}{MN}\sigma^2,
\end{aligned}
$$
(A.7)

B. NMSE for ZF Estimator

The CTF of ZF is redefined as

$$
\hat{\mathbf{h}}_{\mathrm{ZF}} = \mathbf{Z}\mathbf{y} = \mathbf{Z}(\mathbf{X}\mathbf{F}_N\mathbf{g} + \mathbf{w}) = \mathbf{Z}\mathbf{X}\mathbf{F}_N\mathbf{g} + \mathbf{Z}\mathbf{w}.
\tag{B.1}
$$

From (A.1) and (B.1), NMSE for ZF estimator is given as

$$
\begin{aligned}
\mathrm{NMSE}_{\mathrm{ZF}} = {} & \frac{\mathrm{E}\left\{\sum_{n=0}^{N_c/2-1}\left|\left[\hat{h}_{\mathrm{ZF}}\right]_n - [h]_n\right|^2\right\}}{\mathrm{E}\left\{\sum_{n=0}^{N_c/2-1}|x_n|^2 + \sum_{n=N-N_c/2}^{N-1}|x_n|^2\right\}} \\
& + \frac{\mathrm{E}\left\{\sum_{n=N-N_c/2}^{N-1}\left|\left[\hat{h}_{\mathrm{ZF}}\right]_n - [h]_n\right|^2\right\}}{\mathrm{E}\left\{\sum_{n=0}^{N_c/2-1}|x_n|^2 + \sum_{n=N-N_c/2}^{N-1}|x_n|^2\right\}} \\
= {} & \frac{\mathrm{E}\left\{\mathrm{tr}\left\{(\mathbf{F}_N\mathbf{g} + \mathbf{Z}\mathbf{w} - \mathbf{F}_N\mathbf{g})(\mathbf{F}_N\mathbf{g} + \mathbf{Z}\mathbf{w} - \mathbf{F}_N\mathbf{g})^H\right\}\right\}}{N_c} \\
= {} & \frac{\mathrm{E}\left\{\mathrm{tr}\left\{(\mathbf{Z}\mathbf{w})(\mathbf{Z}\mathbf{w})^H\right\}\right\}}{N_c} = \sigma^2,
\end{aligned}
$$
(B.2)

where $\mathrm{tr}\{\cdot\}$ denotes the trace operator.

C. The Noise Suppression Gain by the First Order Linear Interpolation

The pilot symbol interval is a 14-OFDM-symbol in our OFDM system frame format (see Figure 1 and Table 1). The CTF of mth data symbol for a subcarrier, $\hat{h}_m$, can be derived by the first order interpolation method that is given as

$$
\hat{h}_m = \frac{\hat{h}_{p1} - \hat{h}_{p0}}{15}m + \hat{h}_{p0},
\tag{C.1}
$$

where $\hat{h}_{p0}$ and $\hat{h}_{p1}$ are the estimated CTFs of pilot symbols for a subcarrier that has sandwiched data symbols.

Since the noise is included in $\hat{h}_{p0}$ and $\hat{h}_{p1}$ and can be assumed to be independent, the noise suppression gain is calculated as

$$
10 * \log 10\left(\frac{1}{14}\sum_{m=1}^{14}\left\{\left(\frac{m}{15}\right)^2 + \left(\frac{15-m}{15}\right)^2\right\}\right) \approx -1.9\,\mathrm{dB}.
\tag{C.2}
$$

References

[1] H. Atarashi, S. Abeta, and M. Sawahashi, "Variable spreading factor-orthogonal frequency and code division multiplexing (VSF-OFCDM) for broadband packet wireless access," *IEICE Transactions on Communications*, vol. E86-B, no. 1, pp. 291–299, 2003.

[2] P. Hoeher, S. Kaiser, and P. Robertson, "Pilot-symbol-aided channel estimation in time and frequency," in *Proceedings of the IEEE Global Telecommunications Conference (GLOBECOM '97)*, pp. 90–96, Phoenix, Ariz, USA, November 1997.

[3] Y. Li, "Pilot-symbol-aided channel estimation for OFDM in wireless systems," *IEEE Transactions on Vehicular Technology*, vol. 49, no. 4, pp. 1207–1215, 2000.

[4] M. Morelli and U. Mengali, "A comparison of pilot-aided channel estimation methods for OFDM systems," *IEEE Transactions on Signal Processing*, vol. 49, no. 12, pp. 3065–3073, 2001.

[5] G. Auer, A. Dammann, and S. Sand, "Channel estimation for OFDM systems with multiple transmit antennas by exploiting the properties of the discrete Fourier transform," in *Proceedings of the 14th IEEE International Symposium on Personal, Indoor and Mobile Radio Communications (PIMRC '03)*, vol. 2, pp. 1954–1958, Beijing, China, September 2003.

[6] C. Suh, C. S. Hwang, and H. Choi, "Comparative study of time-domain and frequency-domain channel estimation in MIMO-OFDM systems," in *Proceedings of the 14th IEEE International Symposium on Personal, Indoor and Mobile Radio Communications (PIMRC '03)*, vol. 2, pp. 1095–1099, Beijing, China, September 2003.

[7] A. Czylwik, "Adaptive OFDM for wideband radio channels," in *Proceedings of the IEEE Global Telecommunications Conference (GLOBECOM '96)*, vol. 1, pp. 713–718, London, UK, November 1996.

[8] J.-J. van de Beek, O. Edfors, M. Sandell, S. Wilson, and P. Börjesson, "On channel estimation in OFDM systems," in *Proceedings of the 45th IEEE Vehicular Technology Conference (VTC '95)*, vol. 2, pp. 815–819, Chicago, Ill, USA, July 1995.

[9] Y.-H. Yeh and S.-G. Chen, "Efficient channel estimation based on discrete cosine transform," in *Proceedings of IEEE International Conference on Acoustic, Speech, and Signal Processing (ICASSP '03)*, vol. 4, pp. 676–679, Hong Kong, April 2003.

[10] Y. Li, J. H. Winters, and N. R. Sollenberger, "MIMO-OFDM for wireless communications: signal detection with enhanced channel estimation," *IEEE Transactions on Communications*, vol. 50, no. 9, pp. 1471–1477, 2002.